# Toward Optimal Closure of the Earth's Top-of-Atmosphere Radiation Budget

NORMAN G. LOEB,* BRUCE A. WIELICKI,* DAVID R. DOELLING,* G. LOUIS SMITH,+ DENNIS F. KEYES,# SEIJI KATO,* NATIVIDAD MANALO-SMITH,# AND TAKMENG WONG*

*NASA Langley Research Center, Hampton, Virginia
+National Institute of Aerospace, Hampton, Virginia
#Science Systems and Applications, Inc., Hampton, Virginia

(Manuscript received 14 May 2008, in final form 18 July 2008)

ABSTRACT

Despite recent improvements in satellite instrument calibration and the algorithms used to determine reflected solar (SW) and emitted thermal (LW) top-of-atmosphere (TOA) radiative fluxes, a sizeable imbalance persists in the average global net radiation at the TOA from satellite observations. This imbalance is problematic in applications that use earth radiation budget (ERB) data for climate model evaluation, estimate the earth's annual global mean energy budget, and in studies that infer meridional heat transports. This study provides a detailed error analysis of TOA fluxes based on the latest generation of Clouds and the Earth's Radiant Energy System (CERES) gridded monthly mean data products [the monthly TOA/surface averages geostationary (SRBAVG-GEO)] and uses an objective constrainment algorithm to adjust SW and LW TOA fluxes within their range of uncertainty to remove the inconsistency between average global net TOA flux and heat storage in the earth–atmosphere system. The 5-yr global mean CERES net flux from the standard CERES product is 6.5 W m$^{-2}$, much larger than the best estimate of 0.85 W m$^{-2}$ based on observed ocean heat content data and model simulations. The major sources of uncertainty in the CERES estimate are from instrument calibration (4.2 W m$^{-2}$) and the assumed value for total solar irradiance (1 W m$^{-2}$). After adjustment, the global mean CERES SW TOA flux is 99.5 W m$^{-2}$, corresponding to an albedo of 0.293, and the global mean LW TOA flux is 239.6 W m$^{-2}$. These values differ markedly from previously published adjusted global means based on the ERB Experiment in which the global mean SW TOA flux is 107 W m$^{-2}$ and the LW TOA flux is 234 W m$^{-2}$.

## 1. Introduction

The average global net radiation at the top of the atmosphere (TOA) is defined as the difference between the energy absorbed and emitted by the planet. In an equilibrium climate state, the global net radiation at the TOA is zero. In the presence of an increasing climate forcing, an imbalance between the energy absorbed and emitted occurs, and in response the climate system must react to restore the balance (e.g., by changing temperature). The rate at which the earth reacts is modulated by its capacity to store energy. Given that oceans are 10 times more efficient at storing heat than other components of the climate system (e.g., land, ice, atmosphere; Levitus et al. 2001), the global net radiation at the TOA should be in phase with and of similar magnitude as the global ocean heat storage. Wong et al. (2006) showed that this is indeed the case by comparing TOA net flux anomalies from the Earth Radiation Budget Experiment (ERBE) and ocean heat content anomalies from in situ temperature and satellite altimeter data (Willis et al. 2004). Model studies indicate that planetary energy imbalance has grown steadily since the 1960s and that the earth is now absorbing 0.85 ± 0.15 W m$^{-2}$ more solar energy than it radiates to space as heat (see Fig. 1c in Hansen et al. 2005). The model results closely match the Willis et al. (2004) observed ocean heat content change between 1993 and 2003 in the top 750 m of the oceans. Recent results by Köhl and Stammer (2008) indicate that the heating rate during the past decade may be as much as 40% larger than Hansen et al.'s (2005) estimate, mainly because of a larger heat content change in the deep ocean.

As noted by Fasullo and Trenberth (2008), satellite observations of TOA radiation budget show a much larger global net TOA flux imbalance. While the radiances from

*Corresponding author address:* Dr. Norman G. Loeb, Mail Stop 420, NASA Langley Research Center, Hampton, VA 23681-2199.
E-mail: norman.g.loeb@nasa.gov

DOI: 10.1175/2008JCLI2637.1

© 2009 American Meteorological Society

instruments like ERBE and the Clouds and the Earth's Radiant Energy System (CERES) are stable to a few tenths of a W $m^{-2}$ per decade (Loeb et al. 2007a) and provide excellent regional coverage of the distribution of reflected solar and emitted thermal radiation from the earth, the absolute calibration is known to 2% in the shortwave (SW) and 1.5% in the longwave (LW) at the 95% confidence level. Instruments that measure total solar irradiance, such as the Solar Radiation and Climate Experiment (SORCE) instrument (Kopp et al. 2005), are also far more stable than they are absolutely accurate. Consequently, it is not surprising that satellite observations produce larger net TOA flux imbalances than expected.

To use earth radiation budget (ERB) data for climate model evaluation, estimating the earth's annual global mean energy budget (e.g., Kiehl and Trenberth 1997), and in studies that infer meridional heat transports (e.g., Trenberth 1997; Fasullo and Trenberth 2008), one must account for inconsistencies between global long-term average net TOA flux and heat storage within the earth–atmosphere system (Hansen et al. 2005; Willis et al. 2004). Early attempts to adjust ERB TOA fluxes assumed the bulk of the bias in the TOA net flux imbalance is due to sampling and modeling of the diurnal cycle (Trenberth 1997). Consequently, larger adjustments were made in the SW than in the LW (e.g., Kiehl and Trenberth 1997). Recently, Fasullo and Trenberth (2008) adjusted CERES SW and LW TOA fluxes to be consistent with observations of ocean and land heat storage (Willis et al. 2004; Huang 2006) by uniformly increasing outgoing LW TOA flux by 1.5 W $m^{-2}$, and uniformly increasing albedo by $\approx$4% (relative to the original value). The adjustments are meant to account for uncertainties in angular models, scene identification, diurnal sampling, etc. We note, however, that the SW adjustment exceeds the global mean CERES SW TOA flux uncertainty determined in the present study by a factor of $\sim$2.

In this study, we present a detailed summary of the errors and uncertainties that influence the net TOA flux from CERES observations. We focus on the first 5 yr of CERES *Terra* Flight Model 1 (FM1) observations from March 2000 through February 2005. An objective constrainment algorithm is used to adjust SW and LW TOA fluxes within their range of uncertainty to remove the inconsistency between average global net TOA flux and heat storage in the earth–atmosphere system. We also use CERES and Moderate Resolution Imaging Spectrometer (MODIS) measurements to produce a new clear-sky TOA flux climatology that provides TOA fluxes in each region every month. This addresses the long-standing problem of missing regions in clear-sky TOA flux climatologies from coarse spatial resolution instruments like ERBE and CERES. Global monthly mean climatologies of adjusted all-sky and clear-sky SW and LW TOA fluxes are produced for the first 5 yr of CERES *Terra* observations. We refer to this new CERES climatology as CERES-Energy Balanced and Filled (EBAF). CERES-EBAF fluxes are compared with adjusted ERBE fluxes based on previous studies.

## 2. Datasets

This study compares gridded global monthly mean TOA fluxes from the Earth Radiation Budget Experiment (ERBE; Barkstrom 1984), CERES *Terra* (Wielicki et al. 1996), the Global Energy and Water Cycle Experiment (GEWEX) Surface Radiation Budget (SRB) Project (version 2.81, Cox et al. 2006), and the International Satellite Cloud Climatology Project (ISCCP) radiative flux profile dataset (ISCCP-FD product; Zhang et al. 2004). We consider a 5-yr period from March 2000 through February 2005 for all datasets except ERBE. The ERBE data used cover the 3-yr period from February 1986 through January 1989, during which an ERBE scanner simultaneously operated aboard the precessing Earth Radiation Budget Satellite (ERBS) and one of the National Oceanic and Atmospheric Administration (NOAA) polar orbiting satellites (*NOAA-9* or *NOAA-10*).

ISCCP-FD fluxes are from radiative transfer model calculations initialized with visible-infrared imager-based cloud, atmosphere, and surface property retrievals at 3-hourly increments. GEWEX SRB (version 2.81) uses the same visible-infrared satellite measurements and cloud properties as ISCCP but relies on a different set of algorithms to estimate radiative fluxes. Radiative fluxes in the ISCCP-FD and GEWEX SRB data products are described in detail in Zhang et al. (2004) and Cox et al. (2006).

ERBE and CERES radiative fluxes are based upon broadband radiometer measurements that use precision thermistor bolometers (Barkstrom 1984; Wielicki et al. 1996). A detailed description of the algorithms used to determine TOA fluxes from ERBE is provided in Smith et al. (1986), Brooks et al. (1986), and Young et al. (1998). CERES measures filtered radiances in the SW (wavelengths between 0.3 and 5 $\mu$m), total (TOT; wavelengths between 0.3 and 200 $\mu$m), and window (WN; wavelengths between 8 and 12 $\mu$m) regions. To correct for the imperfect spectral response of the instrument, the filtered radiances are converted to unfiltered reflected solar, unfiltered emitted terrestrial LW and WN radiances (Loeb et al. 2001). Since there is no LW channel on CERES, LW daytime radiances are

determined from the difference between the TOT and SW channel radiances.

Three different CERES gridded global monthly mean TOA flux data are considered in this study: CERES ES-4 (ERBE-like, edition2_rev1), the monthly TOA/surface averages (SRBAVG) nongeostationary (nonGEO), and the SRBAVG-geostationary (GEO) edition2D_rev1. The CERES ES-4 uses the same algorithms as ERBE (hence the name ERBE-like) and is intended to ensure continuity between the ERBE and CERES datasets (Wielicki et al. 1996). The SRBAVG-nonGEO and SRBAVG-GEO represent a major advance over ERBE. SRBAVG provides $1° \times 1°$ gridded TOA and surface monthly mean radiative fluxes with consistent cloud and aerosol properties from MODIS. Instantaneous CERES TOA fluxes are estimated from unfiltered radiances using new empirical angular distribution models (ADMs; Loeb et al. 2003a, 2005) that account for variations in surface type, cloud phase (water, ice), cloud fraction, and cloud optical depth inferred from MODIS measurements (Minnis et al. 2003).

Monthly mean cloud properties and radiative fluxes in SRBAVG-nonGEO are determined by spatially averaging the instantaneous values on a $1° \times 1°$ equal-area grid, temporally interpolating at 1-h increments for each hour of every month, and then averaging all hour boxes in a month. SW radiative fluxes between CERES observation times are estimated from the observed fluxes by using scene-dependent diurnal albedo models to estimate how albedo (and therefore flux) changes with solar zenith angle for each local time, assuming the scene properties remain invariant throughout the day. The sun angle–dependent diurnal albedo models used in SRBAVG-nonGEO are based on the CERES ADMs developed for the Tropical Rainfall Measuring Mission (TRMM) satellite (Loeb et al. 2003a). To determine LW fluxes in each hour box between CERES observations, linear interpolation of LW fluxes is used over ocean, whereas daytime and nighttime observations over land and desert are interpolated by fitting a half-sine curve to the observations to account for the much stronger diurnal cycle over land and desert (Young et al. 1998).

To improve cloud property and radiative flux temporal interpolation accuracy, SRBAVG-GEO uses 3-hourly geostationary visible-infrared measurements from five GEO satellites across the globe to account for cloud and radiation changes between CERES observation times. The geostationary data provide the relative shape of the diurnal changes, and CERES provides the absolute reference to anchor the less accurately derived geostationary broadband fluxes. A detailed description of the methodology used to produce SRBAVG-GEO is provided in Doelling et al. (2006), and Keyes et al. (2006) provide validation results.

Another key dataset used in this study is the CERES Single Scanner Footprint TOA/Surface Fluxes and Clouds (SSF) product (Geier et al. 2001; Loeb et al. 2003a). The SSF product merges CERES footprint parameters including time, position, viewing geometry, radiances, and radiative fluxes with coincident information from MODIS, which is used to characterize the clear and cloudy portions of a CERES footprint.

## 3. Global and regional mean TOA fluxes

Table 1 compares 5-yr global mean TOA fluxes from ERBE, CERES *Terra*, GEWEX SRB, and ISCCP-FD. All-sky LW TOA flux shows a range of 4.6 W m$^{-2}$ (235.8 W m$^{-2}$ for ISCCP-FD to 240.4 W m$^{-2}$ for GEWEX SRB), and SW TOA flux shows a range of 8.6 W m$^{-2}$ (96.6 W m$^{-2}$ for SRBAVG-nonGEO Ed2D_rev1 to 105.2 W m$^{-2}$ for ISCCP-FD). While CERES LW TOA fluxes lie in the middle of this range, CERES SW TOA fluxes are $\approx$3 W m$^{-2}$ lower than the other datasets, including ERBE. This $\approx$3 W m$^{-2}$ difference between CERES and ERBE falls just within the 1-$\sigma$ uncertainty in SW channel absolute calibration accuracy of 2% ($\approx$2 W m$^{-2}$) for ERBE and 1% ($\approx$1 W m$^{-2}$) for CERES (Wielicki et al. 1995). Clear-sky TOA fluxes show a range of 5.8 W m$^{-2}$ in the LW (262.3 W m$^{-2}$ for ISCCP-FD to 268.1 W m$^{-2}$ for GEWEX SRB), while the SW range is 5.2 W m$^{-2}$ (49.3 W m$^{-2}$ for CERES ES-4_ED2_rev1 to 54.5 W m$^{-2}$ for GEWEX SRB).

Global mean TOA fluxes from the three CERES products are within 2 W m$^{-2}$ of one another in both the LW and SW. Annual mean regional maps of LW, SW, and net TOA flux differences between CERES ES-4 (ERBE-like) and SRBAVG-nonGEO and between SRBAVG-GEO and SRBAVG-nonGEO are provided in Figs. 1a–f. Since the same CERES radiances are used, the main reason for differences between ES-4 and SRBAVG-nonGEO TOA fluxes (Figs. 1a,c,e) is the ADMs used to infer TOA fluxes: CERES ES-4 TOA fluxes are determined from the same ADMs as those used to process ERBE data, whereas the CERES SRBAVG products use ADMs from Loeb et al. (2005). SW TOA flux differences (Fig. 1c) are largest at mid–high latitudes, reaching 10 W m$^{-2}$. In the LW, ES-4 and SRBAVG-nonGEO differences are largest in the tropics (Fig. 1a), while net TOA flux differences (Fig. 1e) are most pronounced at mid–high latitudes, consistent with the SW TOA flux differences. Because ES-4 reflects so much more solar radiation at mid–high latitudes than SRBAVG-nonGEO, the ES-4 net TOA flux imbalance is 3 W m$^{-2}$ smaller than CERES SRBAVG-nonGEO

TABLE 1. Global mean clear- and all-sky SW, LW, and net TOA radiative fluxes, solar irradiance, and CRE for satellite-based data products (units in W m$^{-2}$).

| Product name | ERBE S-4 | CERES ES-4 Ed2_rev1 | CERES SRBAVG-nonGEO Ed2D_rev1 | CERES SRBAVG-GEO Ed2D_rev1 | GEWEX SRB Version 2.86 | ISCCP FD |
|---|---|---|---|---|---|---|
| Time period | 02/85 – 01/89 | | | 03/00 – 02/2005 | | |
| Solar irradiance | 341.3 | 341.3 | 341.3 | 341.3 | 341.8 | 341.5 |
| LW (All sky) | 235.2 | 239.0 | 237.7 | 237.1 | 240.4 | 235.8 |
| SW (All Sky) | 101.2 | 98.3 | 96.6 | 97.7 | 101.7 | 105.2 |
| Net (All Sky) | 4.9 | 4.0 | 7.0 | 6.5 | −0.3 | 0.5 |
| LW (Clear Sky) | 264.9 | 266.6 | 266.4 | 264.1 | 268.1 | 262.3 |
| SW (Clear Sky) | 53.6 | 49.3 | 51.2 | 51.1 | 54.5 | 54.2 |
| Net (Clear Sky) | 22.8 | 25.4 | 23.7 | 26.2 | 19.2 | 25.0 |
| LW CRE | 29.7 | 27.6 | 28.7 | 27.0 | 27.7 | 26.5 |
| SW CRE | −47.6 | −49.0 | −45.4 | −46.6 | −47.2 | −51.0 |
| NET CRE | −17.9 | −21.4 | −16.7 | −19.7 | −19.5 | −24.5 |

(Table 1). However, this result is fortuitous and does not imply that ES-4 is more accurate than SRBAVG-nonGEO.

Loeb et al. (2007b) used a rigorous validation strategy to show that the overall bias in global monthly mean TOA flux due to uncertainties in the CERES ADMs is less than 0.2 W m$^{-2}$ in the SW and 0.2–0.4 W m$^{-2}$ in the LW. Furthermore, fluxes from the ERBE ADMs show systematic dependencies on viewing geometry (Suttles et al. 1992) and cloud type that are largely absent when CERES ADMs are used (Loeb et al. 2003b, 2006). In addition, the viewing zenith angle–dependent biases in ERBE-like fluxes are more pronounced at mid–higher latitudes, further increasing the likelihood that ES-4 fluxes are overestimated in these regions.

Differences between CERES SRBAVG-nonGEO and SRBAVG-GEO all-sky TOA fluxes are due to temporal interpolation differences. Explicitly accounting for diurnal variations in clouds and the associated radiative fluxes causes global mean TOA fluxes from SRBAVG-GEO to be lower than SRBAVG-nonGEO by 0.6 W m$^{-2}$ in the LW and 1.1 W m$^{-2}$ larger in the SW (Table 1). The LW difference is primarily due to land convection peaking near sunset between *Terra* overpasses, which are at 10:30 a.m. and 10:30 p.m. local time. SW TOA flux differences are much larger at regional scales (Fig. 1d), reaching magnitudes of 20–30 W m$^{-2}$ in stratus regions off the coasts of the Americas and Africa, as well as in land convective areas.

CERES clear-sky monthly mean TOA fluxes are provided for 1° × 1° latitude–longitude regions derived from CERES footprints that are completely cloud-free according to 1-km resolution MODIS data (Minnis et al. 2003). Global mean SRBAVG-nonGEO and SRBAVG-GEO clear-sky SW TOA fluxes are based on very similar algorithms and therefore are within 0.1 W m$^{-2}$ of one another. In the LW, independent algorithms are used. The SRBAVG-nonGEO mean clear-sky LW flux exceeds the SRBAVG-GEO value by 2.3 W m$^{-2}$, much larger than expected. The difference is associated with errors in SRBAVG-GEO. In overcast ocean regions, the GEO cloud retrieval misidentifies a small fraction of all the regional pixels as clear sky. These misidentified pixels have a large impact, as there are few CERES clear-sky observations to begin with. Over land, the GEO-derived broadband radiance is underestimated near sunrise because of limitations of the global GEO narrowband-to-broadband parameterization, which is independent of scene type. For the next release (edition 3), a narrow-to-broadband relationship is being developed that will take scene type into account. Since the GEO LW fluxes are normalized to the CERES fluxes at *Terra* (10:30 a.m.) sampling times, the sunrise and sunset time periods may be biased because of narrow-to-broadband radiance conversion errors. As these are known GEO algorithm deficiencies, the nonGEO LW clear sky are likely to be more accurate.

Because of the large variation in SW and LW TOA fluxes amongst the datasets considered in Table 1, there is a marked 7.3 W m$^{-2}$ range in all-sky net TOA flux. GEWEX SRB shows a negative net TOA flux (−0.3 W m$^{-2}$), while all other values are positive. The largest imbalance is for the SRBAVG-nonGEO, which shows a net TOA flux of 7 W m$^{-2}$. Accounting for diurnal variations in cloud properties reduces this by only 0.5 W m$^{-2}$. While such a large net TOA flux imbalance is unphysical, it is unclear from Table 1 whether or not it can be explained by uncertainties in the measurements and algorithms that are used to determine the TOA fluxes. To address this question, the following section

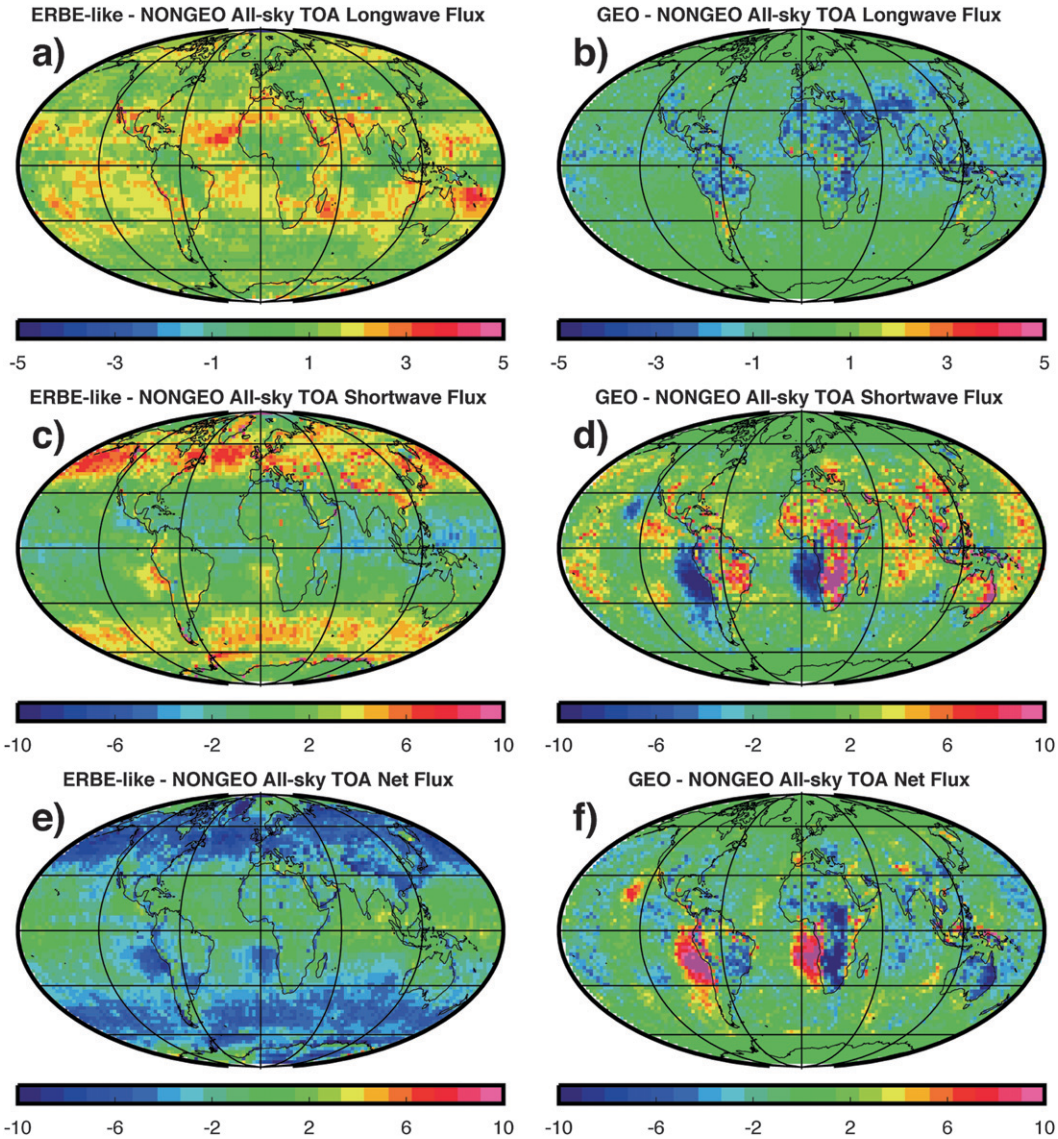


FIG. 1. Annual mean TOA flux difference between (left) CERES ERBE-like and CERES SRBAVG-nonGEO and (right) CERES SRBAVG-nonGEO and SRBAVG-GEO for (a), (b) LW; (c), (d) SW; and (e), (f) net for the year 2002.

provides a detailed error analysis of the SRBAVG-GEO global mean fluxes.

## 4. Uncertainties in global mean TOA fluxes

Table 2 provides a summary of the uncertainty associated with global mean SW, LW, and net TOA fluxes from SRBAVG-GEO. Sources of uncertainty are divided into two categories: bias errors of known sign and bias errors of unknown sign. According to recent measurements by the Total Irradiance Monitor (TIM) aboard the SORCE satellite, the annual average solar irradiance at the TOA and $2\sigma$ uncertainty is 1361 $\pm$ 0.8 W m$^{-2}$ (Kopp et al. 2005). This is approximately 4 W m$^{-2}$ lower than what is assumed in SRBAVG-GEO to determine net TOA flux, which is based on solar irradiance measurements from missions prior to SORCE. Averaged over the globe, the 4 W m$^{-2}$ difference between SORCE-TIM solar irradiance and the assumed SRBAVG-GEO value corresponds to $+1 \pm 0.2$ W m$^{-2}$ in net TOA flux. We assume the SORCE-TIM value is correct and the SRBAVG solar irradiance has bias of $+1$ W m$^{-2}$.

The question of whether the solar irradiance is 1361 W m$^{-2}$ or is closer to 1365 W m$^{-2}$ is a topic of much recent debate within the solar radiation community. A

TABLE 2. Bias errors for SRBAVG-GEO global mean fluxes. Numbers in parentheses correspond to clear sky.

| | Bias errors of known sign (W m$^{-2}$) | | | | |
|---|---|---|---|---|---|
| Error source | Incoming solar | Outgoing SW | Outgoing LW | Net incoming | Comment |
| Total solar irradiance | +1 | 0 | 0 | +1 | Recent solar irradiance measurement vs assumed solar irradiance in CERES |
| Spherical earth assumption | +0.29 | +0.18 (+0.11) | −0.05 (−0.06) | +0.16 (+0.24) | Weighting latitude zones in geocentric vs geodedic coordinates. |
| Near-terminator flux | 0 | −0.3 | 0 | +0.3 (+0.15) | Discretization uncertainty in time–space averaging algorithm at $\theta_o > 85°$ |
| Heat storage | 0 | 0 | 0 | +0.85 | Hansen et al. (2005) |
| | Bias errors of unknown sign (W m$^{-2}$) | | | | |
| Source | Incoming solar | Outgoing SW | Outgoing LW | Net incoming | Comment |
| Total solar irradiance | ±0.2 | 0 | 0 | ±0.2 | Absolute calibration (95% confidence) |
| Filtered radiance | 0 | ±2.0 | ±2.4 (N)<br>±5.0 (D) | ±4.2 | Absolute calibration (95% confidence) |
| Unfiltered radiance | 0 | ±0.5 | ±0.25 (N)<br>±0.45 (D) | ±1.0 | - Instrument spectral response function<br>- Unfiltering algorithm |
| Radiance-to-flux conversion | 0 | ±0.2 | ±0.3 | ±0.4 | Angular distribution model error |
| Flux reference level | 0 | ±0.1 | ±0.2 | ±0.2 | Uncertainty in assuming a 20-km reference level |
| Time & space averaging | 0 | ±0.3 | ±0.3 | ±0.4 | Geostationary instrument normalization with CERES |
| Heat storage | 0 | 0 | 0 | ±0.15 | Hansen et al. (2005) |
| | Expected range in net TOA flux: −2.1 W m$^{-2}$ to 6.7 W m$^{-2}$ | | | | |

workshop in 2005 at the National Institute of Standards and Technology (NIST) partially explained the reasons for the discrepancies (Butler et al. 2008). Based on intra-instrument cavity comparisons, the report notes that some of the instruments have underestimated their uncertainty (TIM was not one of them). It points out that part of the reason for the difference between TIM and the other instruments is associated with the optical design of the instruments. For example, most instruments place a view-limiting aperture near the front of the instrument and a precision aperture close to the cavity. Only TIM reverses this order by placing a narrow precision aperture at the front and a view-limiting aperture near the cavity. As a result, TIM minimizes the amount of scattered light in the instrument that can erroneously increase the signal. Another important factor is diffraction. Most instruments prior to TIM did not make a correction for light diffracted into the cavity. When a diffraction correction is applied to the three Active Cavity Radiometer Irradiance Monitors (ACRIMs), the solar irradiance is reduced by as much as 1.8 W m$^{-2}$. While these explanations do not account for the entire 4 W m$^{-2}$ difference in solar irradiance, they do suggest that measurements from several older instruments are too high and that they get closer to TIM when the appropriate corrections are made.

Another positive bias is associated with how the global average solar irradiance is calculated. It is common practice to assume a spherical earth when averaging TOA insolation over the earth's surface. This gives the well-known $S_o/4$ expression for mean solar irradiance, where $S_o$ is the instantaneous solar irradiance at the TOA. When a more careful calculation is made by assuming the earth is an oblate spheroid instead of a sphere, and the annual cycle in the earth's declination angle and the earth–sun distance are taken into account, the division factor becomes 4.0034 instead of 4. The spherical earth assumption causes a + 0.29 W m$^{-2}$ bias in net TOA flux. Similarly, assuming a spherical earth in determining the global average SW and LW TOA fluxes (by using a latitude weighting in geocentric instead of geodedic coordinates) results in +0.18 and −0.05 W m$^{-2}$ biases, respectively.

Another TOA flux bias error is associated with the manner in which TOA fluxes near the terminator are determined in SRBAVG-GEO. TOA fluxes at solar

zenith angles between 85° and 90° are estimated by linearly extrapolating albedos (from diurnal albedo models) at solar zenith angles 75° and 85° and converting these to fluxes. To estimate the error, the TOA flux at a 90° solar zenith angle is determined from instantaneous CERES-TRMM radiances and an independent estimate of the near-terminator flux is derived (Kato and Loeb 2003). On a global annual average, the SRBAVG extrapolation is found to underestimate the SW flux by 0.3 W $m^{-2}$, corresponding to a + 0.3 W $m^{-2}$ bias in net TOA flux.

The largest uncertainty in determining TOA radiation budget from satellite is associated with the absolute calibration of the instrument. The CERES absolute calibration uncertainty is ±2% in the SW channel and ±1% in the TOT channel, at the 95% confidence level (Priestley et al. 2002). As explained in more detail in the appendix, this accounts for up to 4.2 W $m^{-2}$ of the 6.5 W $m^{-2}$ net TOA flux imbalance in the SRBAVG-GEO product. In addition to absolute calibration uncertainty, one must also account for uncertainties in the instrument spectral response function and the conversion of measured CERES filtered radiances to unfiltered radiances. In the SW, errors are estimated to be ±0.5 W $m^{-2}$ based on comparisons of CERES *Terra* and CERES *Aqua* TOA flux anomalies (Loeb et al. 2007a). LW unfiltering errors at night are ±0.25 W $m^{-2}$, while daytime unfiltering errors are larger since both the TOT and SW channels are used to determine unfiltered LW. To estimate the error, we assume that uncertainties in the spectral response function for the SW and LW portions of the TOT channel and the SW channel are uncorrelated. This leads to an uncertainty in daytime LW radiance of ±0.45 W $m^{-2}$. Radiance-to-flux uncertainties due to ADM errors are ±0.2 W $m^{-2}$ in the SW and ±0.3 W $m^{-2}$ LW (Loeb et al. 2007b). Since TOA flux represents a flow of radiant energy per unit area, and varies with distance from the earth according to the inverse-square law, a reference level is also needed to define satellite-based TOA fluxes. From theoretical radiative transfer calculations using a model that accounts for spherical geometry, Loeb et al. (2002) showed that the optimal reference level for defining TOA fluxes in radiation budget studies is 20 km. Although the optimal flux reference level depends slightly on scene type because of differences in effective transmission of solar radiation with cloud height, the difference in flux caused by neglecting the scene-type dependence is less than 0.1%, which corresponds to approximately ±0.1 W $m^{-2}$ in the SW and ±0.2 W $m^{-2}$ in the LW. To estimate errors in time and space interpolation, we compare SRBAVG-GEO minus SRBAVG-nonGEO differences between *Terra* and *Aqua* ($\Delta F_{\mathrm{Terra}} - \Delta F_{\mathrm{Aqua}}$, where $\Delta = F_{\mathrm{GEO}} - F_{\mathrm{nonGEO}}$) and assume that all of this difference is caused by time–space averaging errors. This yields a ± 0.3 W $m^{-2}$ uncertainty in both SW and LW.

When all of these errors in solar irradiance, SW and LW TOA flux are combined, and the 0.85 ± 0.15 W $m^{-2}$ of heat storage by the earth–atmosphere is included (Hansen et al. 2005), the possible range of net TOA flux becomes −2.1 to 6.7 W $m^{-2}$, which bounds the 6.5 W $m^{-2}$ SRBAVG-GEO net TOA flux in Table 1.

## 5. TOA flux adjustments

To remove the inconsistency between average global net TOA flux and heat storage in the earth–atmosphere system, we use an objective constrainment algorithm (section 5a) and the uncertainty ranges presented in Table 2 to derive optimal adjustments to the SRBAVG-GEO incoming solar, SW, and LW TOA fluxes. After removing the constant flux bias errors in Table 2, the constrainment algorithm assigns errors to each error source listed in Table 2, accounting for the assessed range of uncertainty in each term and the overall difference between the average global net and the assumed heat storage in the earth–atmosphere system. We assume the "true" global net flux imbalance during the CERES period considered is +0.85 W $m^{-2}$, based on Hansen et al. (2005). The optimal adjustments are applied to SRBAVG-GEO to produce all-sky CERES-EBAF TOA fluxes.

After the release of SRBAVG-GEO edition 2D, an error was discovered in the computation of the declination angle and earth–sun distance factor. The angle and factor were computed at 0000 UTC instead of 1200 UTC, which is appropriate for computing the solar incoming in local time. This has no effect on the annual mean insolation but significantly affects the monthly zonal solar incoming fluxes near the poles. This error is corrected in the final adjusted TOA fluxes and will also be rectified in the next SRBAVG version (edition 3). Adjustments to total solar irradiance associated with the spherical earth assumption are applied zonally to improve the accuracy of incoming solar radiation at each latitude. While these adjustments are applied at the zonal level, the globally averaged correction is the same as in Table 2. Similarly, adjustments in SW TOA fluxes due to near-terminator flux biases are also applied zonally without modifying the global mean. Separate adjustments are made for clear and all-sky TOA fluxes.

TABLE 3. Net flux sensitivity ($a_i$), standard deviation of error ($\sigma_i$), maximum likelihood error ($x_i$), and error effect on net TOA flux.

| Parameter | Net TOA flux sensitivity, $a_i$ (W m$^{-2}$ %$^{-1}$) | $2\sigma$ uncertainty, $\delta_\iota$ (%) | Maximum likelihood solution, $x_i$ (%) | TOA flux adjustment (W m$^{-2}$) |
|---|---|---|---|---|
| SW gain | −0.977 | 2.0 | 1.6 | 1.57 |
| LW gain | −2.37 | 1.0 | 0.972 | 2.3 |
| Unfiltered SW | −0.977 | 0.5 | 0.105 | 0.1 |
| Unfiltered LW (N) | −1.19 | 0.2 | 0.022 | 0.03 |
| Unfiltered LW (D) | −1.19 | 0.38 | 0.07 | 0.08 |
| SW radiance to flux | −0.977 | 0.20 | 0.017 | 0.02 |
| LW radiance to flux | −2.37 | 0.13 | 0.016 | 0.04 |
| Time-averaging SW | −0.977 | 0.30 | 0.038 | 0.04 |
| Time-averaging LW | −2.37 | 0.13 | 0.016 | 0.04 |
| Reference level, SW | −0.977 | 0.10 | 0.004 | 0.00 |
| Reference level, LW | −2.37 | 0.08 | 0.007 | 0.02 |
| Incoming solar | 3.40 | 0.06 | −0.005 | −0.02 |
| Total SW | | | | 1.7 |
| Total LW | | | | 2.5 |
| Total net | | | | −4.2 |

### *a. Constrainment algorithm*

The global average net TOA flux is expressed as follows:

$$R_N = E_o - (F^{\mathrm{SW}} + F^{\mathrm{LW}}), \tag{1}$$

where $E_o$ is the annual mean solar insolation at the TOA averaged over the globe and $F^{\mathrm{SW}}$ and $F^{\mathrm{LW}}$ are the global average SW and LW TOA fluxes. If the earth were in radiative balance for the annual mean, $R_N$ would be zero. However, given a warming trend, there is a net imbalance because of heat storage within the earth–atmosphere system. There are also errors in the computed $E_o$, $F^{\mathrm{SW}}$, and $F^{\mathrm{LW}}$ because of measurement errors and there are errors in computing $R_N$ from the measurements. Thus,

$$R_N = H + \varepsilon_{R_N}, \tag{2}$$

where $H$ is the global average heat storage and $\varepsilon_{R_N}$ is the error in $R_N$ arising because of uncertainties in several factors $p_i$ involved in determining $R_N$ (e.g., instrument calibration, unfiltering, radiance-to-flux conversion, etc.). We wish to modify the parameters $p_i$ by some amount $x_i$ such that the revised $R_N$ is equal to $H$. That is,

$$\hat{R}_N = R_N + \sum_i \frac{\partial R_N}{\partial p_i} x_i = H. \tag{3}$$

This requires finding $x_i$ such that

$$\sum_i \frac{\partial R_N}{\partial p_i} x_i = -\varepsilon_{R_N}. \tag{4}$$

Let $a_i = \frac{\partial R_N}{\partial p_i}$ denote the partial derivatives of global mean net flux with respect to each parameter $p_i$, and represent $x_i$ and $a_i$ as vectors $\mathbf{x}$ and $\mathbf{a}$, so that Eq. (4) may be written as

$$\mathbf{a}^{\mathbf{t}}\mathbf{x} = -\varepsilon_{R_N}. \tag{5}$$

We have one equation with $N$ unknowns, where $N$ is the number of parameters to adjust. The criterion for selecting these parameters is to choose the most likely set of parameters $x_i$ that satisfy Eq. (5) using a maximum likelihood estimate for the $x_i$. The following assumptions are made: (i) $x_i$ has mean 0 for all $i$; (ii) all $x_i$'s are normally distributed. With these assumptions the probability distribution can be written as

$$P\{\mathbf{x}\} = (2\pi)^{-n/2}[\det(\mathbf{C})]^{-1/2}\exp(-\mathbf{x}^{\mathbf{t}}\mathbf{C}^{-1}\mathbf{x}/2), \tag{6}$$

where $\mathbf{C}$ is the covariance matrix of the errors. The most likely set of errors is given by maximizing the probability $P(\mathbf{x})$, which is equivalent to minimizing the exponent subject to the constraint of Eq. (5). This is done by the method of Lagrangian multipliers, whereby we minimize

$$\Omega = \tfrac{1}{2}\mathbf{x}^{\mathbf{t}}\mathbf{C}^{-1}\mathbf{x} + \lambda\mathbf{a}^{\mathbf{t}}\mathbf{x}, \tag{7}$$

where $\lambda$ is the Lagrangian multiplier. The maximum likelihood solution is

$$\mathbf{x} = -\lambda\mathbf{C}\mathbf{a}. \tag{8}$$

This result is used with Eq. (5), whence

$$\lambda = (\mathbf{a}^{\mathbf{t}}\mathbf{C}\mathbf{a})^{-1}\varepsilon_{R_N}. \tag{9}$$

TABLE 4. Global mean (March 2000–February 2005) clear- and all-sky SW, LW, and net TOA radiative fluxes, solar irradiance, and CRE for adjusted ERBE (all sky only) and CERES fluxes. CERES-EBAF corresponds to "Energy Balanced and Filled" and accounts for adjustments in both clear and all sky (units in W m$^{-2}$).

| | Adjusted ERBE (February 1985–April 1989) | Adjusted ERBE (February 1985–April 1989) | Adjusted CERES (March 2000–May 2004) | Adjusted CERES (this study; March 2000–February 2005) | | |
|---|---|---|---|---|---|---|
| Product name | Trenberth (1997) | Fasullo and Trenberth (2008) | Fasullo and Trenberth (2008) | CERES SRBAVG-nonGEO Ed2D_rev1 | CERES SRBAVG-GEO Ed2D_rev1 | CERES-EBAF TOA |
| Solar irradiance | 341.3 | 341.3 | 341.3 | 340.0 | 340.0 | 340.0 |
| LW (all sky) | 234.4 | 234.4 | 238.5 | 240.2 | 239.6 | 239.6 |
| SW (all sky) | 106.9 | 106.9 | 101.9 | 98.4 | 99.5 | 99.5 |
| Net (all sky) | 0.0 | 0.0 | 0.9 | 1.38 | 0.85 | 0.85 |
| LW (clear sky) | 264.9[a] | 264.9[a] | 269.1[b] | 269.2 | 266.9[c] | 269.1 |
| SW (clear sky) | 53.6[a] | 53.6[a] | 52.9[b] | 52.1 | 52.0 | 52.9 |
| Net (clear sky) | 22.8[a] | 22.8[a] | 18.0[b] | 18.7 | 21.1 | 18.0 |
| LW CRE | 30.5[a] | 30.5[a] | 30.6[b] | 29.0 | 27.3 | 29.5 |
| SW CRE | −53.3[a] | −53.3[a] | −49.0[b] | −46.3 | −47.5 | −46.6 |
| Net CRE | −22.8[a] | −22.8[a] | −18.4[b] | −17.3 | −20.2 | −17.1 |

[a] ERBE clear-sky fluxes are from Table 1 and have not been adjusted.
[b] Adjusted clear-sky CERES fluxes derived in this study are assumed.
[c] The large difference between SRBAVG-nonGEO and SRBAVG-GEO mean clear-sky LW flux is due to misidentification of some overcast scenes as clear in SRBAVG-GEO (section 3).

Equations (8) and (9) give $N + 1$ equations in the $N$ $x_i$'s and $\lambda$ such that the $x_i$'s are the most likely values of errors in the measurement and data product generation for which the global net radiation is equal to the global average heat storage. Further discussion of the method is given by Smith (2008).

Application of the constrainment algorithm is shown in Table 3. Errors due to 12 parameters are considered. The net TOA flux sensitivities ($a_i$'s) are given as the change in net TOA flux for a percentage change in a given quantity. For example, an increase in SW TOA flux of 1% results in a 0.977 W m$^{-2}$ decrease in net TOA flux, so $a_i$ = -0.977 W m$^{-2}$ %$^{-1}$. For the present application, the errors in the various terms are assumed to be uncorrelated, so that the covariance matrix **C** is diagonal. From Eq. (9), the Lagrangian multiplier becomes

$$\lambda = \frac{\varepsilon_{R_N}}{\sum_i a_i^2 \delta_i^2}, \tag{10}$$

where $\delta_i$ is the uncertainty in the $i$th parameter. After removing the biases of known sign (Table 2), the remaining net TOA flux imbalance ($\varepsilon_{R_N}$) is 4.2 W m$^{-2}$ and the Lagrangian multiplier is $\lambda = 0.41$ W$^{-1}$ m$^2$. The maximum likelihood solution is then determined from

$$x_i = -\lambda a_i \delta_i^2. \tag{11}$$

### b. Results of constrainment procedure

Table 3 provides $x_i$ (in percent) and the corresponding TOA flux adjustment (in W m$^{-2}$) associated with each error source. Approximately, 90% of the adjustment (after removing biases of known sign in Table 2) is associated with uncertainties in absolute calibration. The remaining 10% is associated with radiance unfiltering, radiance-to-flux conversion and time–space averaging.

The final adjusted global mean SW, LW, and net TOA fluxes are determined by subtracting the biases of known sign in Table 2 from the original SRBAVG-GEO fluxes and adding the adjustments at the bottom of Table 3. The column labeled "CERES-EBAF" in Table 4 provides the final adjusted values. The global mean SW TOA flux is 99.5 W m$^{-2}$, corresponding to an albedo of 0.293. This represents an increase in SW TOA flux of 1.8 W m$^{-2}$ (1.8%) compared to SRBAVG-GEO Ed2D_rev1 (Table 1). The global mean LW TOA flux is 239.6 W m$^{-2}$, which corresponds to a 2.5 W m$^{-2}$ (1.0%) increase compared to SRBAVG-GEO Ed2D_rev1. These changes, together with a decrease in solar irradiance of 1.3 W m$^{-2}$ (340 W m$^{-2}$ instead of 341.3 W m$^{-2}$), result in an imbalance of ~0.9 W m$^{-2}$, consistent with Hansen et al. (2005). Fasullo and Trenberth (2008) arrived at the same net TOA flux imbalance by increasing SW 4.2 W m$^{-2}$ (4.3%), LW by 1.4 W m$^{-2}$ (0.6%), and leaving the mean solar irradiance unchanged.

The SW adjustment in Fasullo and Trenberth (2008) exceeds the global mean CERES SW TOA flux uncertainty (Table 2) by a factor of ~2.

Differences between adjusted ERBE (Fasullo and Trenberth 2008) and CERES-EBAF fluxes in Table 4 are especially noteworthy: the ERBE SW flux is 7.4 W $m^{-2}$ larger than CERES-EBAF while the ERBE LW TOA flux is lower by 5.2 W $m^{-2}$. Figure 2 provides a direct comparison of adjusted ERBE and CERES-EBAF SW, LW, and net TOA fluxes as well as the calculated solar irradiance used in both products. Fasullo and Trenberth (2008) produced an update to the previous Trenberth (1997) adjusted ERBE fields by accounting for the discontinuity resulting from the loss of *NOAA-9* in January 1987 and in the implied transport of energy from land to ocean regions based on ERBS retrievals.

ERBE adjusted SW TOA fluxes exceed CERES-EBAF values by 10 W $m^{-2}$ at low latitudes, and reach a maximum difference of 30 W $m^{-2}$ near 80°N during June (Fig. 2a). In the LW, adjusted ERBE fluxes are generally lower than CERES-EBAF by 2.5–7.5 W $m^{-2}$ and the differences have a weaker latitude dependence than in the SW. Differences in net TOA flux are most pronounced between 70° and 90°N for May and July, reaching −25 W $m^{-2}$ (Fig. 2c).

Because the anisotropies of snow and sea ice are so different than those of land and water, failure to correctly identify clear-sky snow and sea ice from cloud leads to large TOA flux errors at high latitudes in the ERBE data. The ERBE processing uses monthly snow/ice maps derived from passive microwave observations (Coleman et al. 1997), and clear and cloudy scenes are identified using 40-km ERBE broadband radiance measurements by applying a maximum likelihood estimation technique (Wielicki and Green 1989). Li and Leighton (1991) compared ERBE scene identification with that derived using improved snow/sea ice maps and imager-based cloud/clear-sky scene identification at high latitudes during summer. They found considerable errors in both ERBE snow/sea ice boundaries and in ERBE clear/cloud identification. CERES improves scene discrimination at high latitudes by using daily maps of snow and sea ice fraction provided by the National Snow and Ice Data Center (Hollinger et al. 1990; Cavalieri et al. 1990; Comiso 1990). These maps are based on Special Sensor Microwave Imager (SSM/I) measurements at a resolution of 25 by 25 km. Improvements in cloud/clear-sky discrimination in CERES footprints is obtained by using high spatial resolution MODIS measurements (Minnis et al. 2003). Kato and Loeb (2005) used the improved scene identification to develop new ADMs for CERES footprints with snow and sea ice. They estimated the mean relative albedo error due to ADM uncertainties to be ~0.1% for all scene types except thin sea ice, where the estimated relative albedo error is 1%.

Figure 2d shows systematic differences in TOA solar irradiances in April and August at high latitudes in the Northern Hemisphere, and in February and October at high latitudes in the Southern Hemisphere. The differences reach 10 W $m^{-2}$ between 85° and 90° latitude. These differences are due to differences in the computation of the declination angle and earth–sun distance factor: ERBE computed declination and earth–sun distance at 1200 UTC from the previous day, whereas the CERES-EBAF fluxes correctly use 1200 UTC from the current day.

## 6. High-resolution clear-sky fluxes

As noted earlier, CERES SRBAVG clear-sky monthly mean TOA fluxes are provided for 1° × 1° latitude–longitude regions derived from CERES footprints that are completely cloud free according to 1-km-resolution MODIS data. Because of the coarse spatial resolution of CERES (20 km at nadir), this approach only considers flux contributions from cloud-free regions occurring over relatively large spatial scales and meteorological conditions and geographical regions where clouds occur less frequently. As a result, clear-sky maps from CERES SRBAVG contain many missing regions. Furthermore, ignoring clear-sky contributions occurring at spatial scales smaller than a CERES footprint could potentially bias the mean clear-sky fluxes and estimates of the radiative effects of clouds (obtained from clear-sky and all-sky flux differences). We introduce an alternative approach that attempts to recover clear-sky flux contributions at smaller spatial scales. This approach is an extension of that used by Loeb and Manalo-Smith (2005) to estimate the SW TOA direct radiative effects of aerosols over ocean. The Geostationary Radiation Budget (GERB) experiment uses a similar approach to infer clear-sky fluxes in coarse-resolution GERB footprints (Dewitte et al. 2008). We determine gridbox mean clear-sky fluxes using an area-weighted average of (i) CERES broadband fluxes from completely cloud-free footprints, and (ii) MODIS-derived "broadband" clear-sky fluxes estimated from the cloud-free portions of partly and mostly cloudy CERES footprints. In both cases, clear regions are identified using the CERES cloud algorithm applied to MODIS pixel data (Minnis et al. 2003). Clear-sky fluxes in partly and mostly cloudy CERES footprints are derived using MODIS–CERES narrow-to-broadband regressions to convert MODIS narrowband radiances averaged over the clear portions

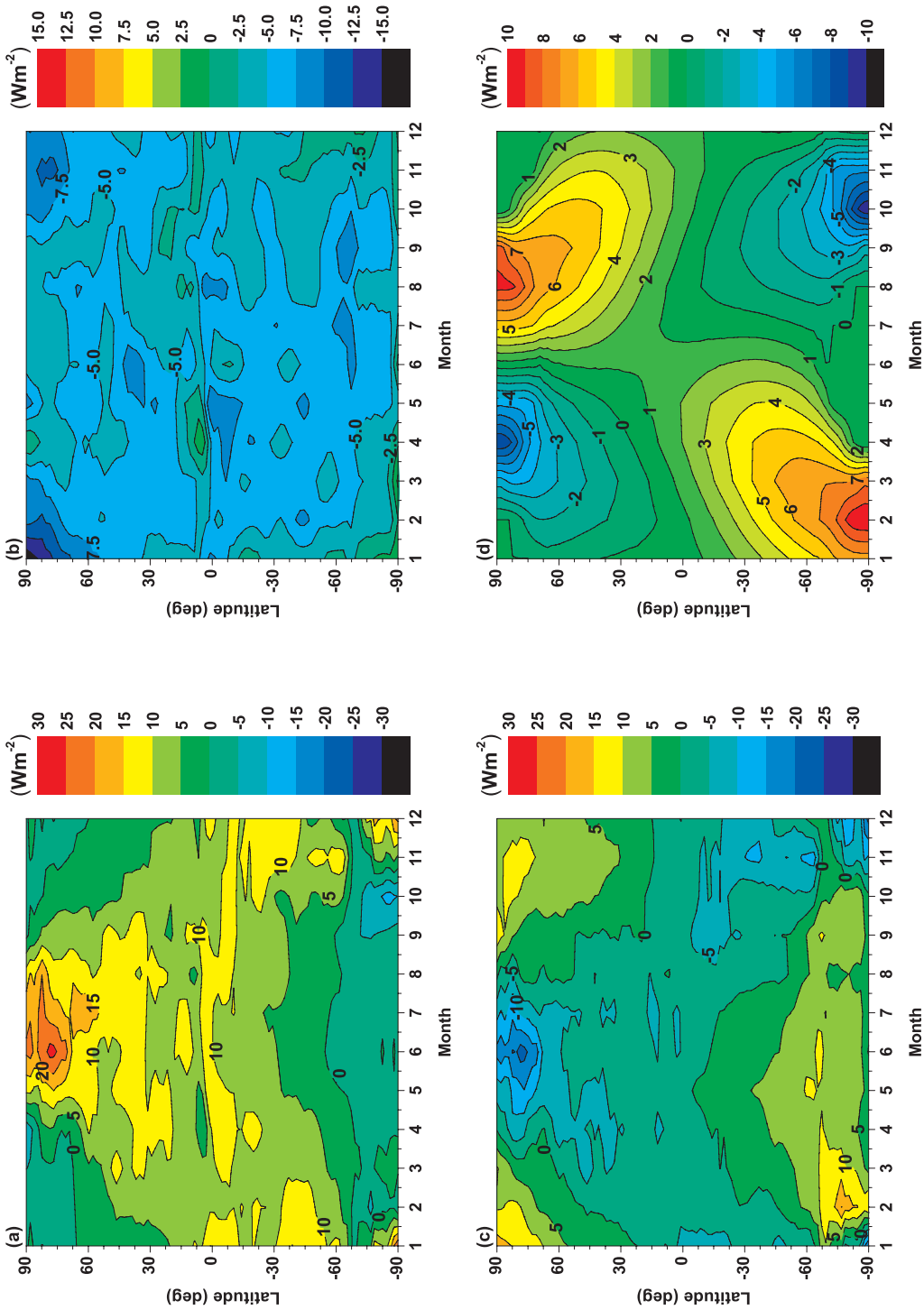


FIG. 2. Difference in (a) SW TOA flux, (b) LW TOA flux, (c) net TOA flux, and (d) solar irradiance between adjusted ERBE and adjusted CERES climatologies (ERBE minus CERES).

of a footprints to broadband SW radiances. The "broadband" MODIS radiances are then converted to TOA radiative fluxes using CERES clear-sky ADMs (Loeb et al. 2005). To convert MODIS narrowband radiance measurements to a broadband radiance estimate ($\hat{I}_{BB}$), the following expression is used:

$$\hat{I}_{BB} = a_0 + \sum_{i=1}^{N_\lambda} a_i I_i, \tag{8}$$

where the $a_i$'s are regression coefficients, and the $I_i$'s correspond to narrowband MODIS radiances in $N_\lambda$ channels. The regression coefficients are determined monthly by relating CERES radiances in cloud-free footprints with coincident MODIS narrowband radiances. In the SW, a three-channel narrow-to-broadband regression is developed between clear-sky CERES SW radiances and MODIS radiances at 0.645, 0.858, and 1.632 $\mu$m. Separate regressions are developed for ocean, forests, savannahs, grasslands, and dark and bright deserts, as defined in Loeb et al. (2003a). The regression relations are stratified according to viewing geometry in discrete intervals of solar zenith angle (10° increments), viewing zenith angle (10° increments), and relative azimuth angle (20° increments). In the LW, broadband radiances are regressed against MODIS radiances at 11 $\mu$m for each month. Separate LW regression relations are derived for daytime and nighttime conditions. The LW regressions are defined for the same surface types as in the SW and are provided as a function of viewing zenith angle only in 10° increments. To account for variations in column water vapor, the LW regressions are also defined as a function of precipitable water for the following intervals: $< 1$, 1–3, 3–5, and $> 5$ cm. Over water, precipitable water is obtained from SSM/I retrievals; over land and desert, it is obtained from meteorological values (Suarez 2005).

Figures 3a,b show the regional distribution of the relative bias error in SW and LW flux due to the narrow-to-broadband conversion for March 2002 when the narrow-to-broadband regressions are applied to cloud-free CERES footprints. Relative bias errors are generally smaller than 1% in the SW except over ocean between 0° and 30°S where the narrow-to-broadband regressions underestimate the CERES SW radiances by up to 4%–5%. Over land, positive SW relative bias errors exceed 4% over central and southern parts of South America and over South Africa. LW relative bias errors are generally $< 1\%$ except over the North Atlantic Ocean and part of the Indian Ocean. To minimize the influence of narrow-to-broadband regression errors such as those in Figs. 3a,b on the final monthly mean clear-sky flux in a grid box, the mean clear-sky flux contribution from all partly and mostly cloudy footprints is adjusted to correct for the narrow-to-broadband error prior to computing the final gridbox mean clear-sky flux. This adjustment is made monthly for each grid box. If a grid box has no narrow-to-broadband error assigned to it, a value is inferred by averaging the error in neighboring grid boxes (weighted by the distance between the grid boxes).

Mean clear-sky MODIS–CERES fluxes based on this new approach are shown in Figs. 3c,d for March 2002. Because high-resolution MODIS data are used, clear-sky fluxes are available in all grid boxes; in contrast, CERES clear-sky maps have several grid boxes with missing values. Differences between MODIS–CERES and CERES-only clear-sky fluxes are shown in Figs. 3e,f. On average, the MODIS–CERES clear-sky fluxes exceed the CERES-only values by 0.9 $Wm^{-2}$ in the SW, and are smaller than CERES-only values in the LW by 0.3 $Wm^{-2}$. The increase in clear-sky SW flux for the MODIS–CERES approach can be explained by increases in aerosol optical depth in the vicinity of clouds caused by aerosol swelling in response to the higher relative humidity environment, an increase in particle production near clouds, and possibly an increase in aerosol size caused by in-cloud processing (Matheson et al. 2006). The reason LW fluxes decrease is likely due to the differences in temperature and humidity profiles near clouds compared to extensive cloud-free regions. Another possible cause for the increased SW and decreased LW MODIS–CERES clear-sky fluxes is cloud contamination. As the true cloud cover increases in a region, misclassification of cloudy pixels as clear may increase, especially in trade-cumulus regions where clouds are low (and therefore have little thermal contrast with the surface) and often occur at spatial scales well below the nominal 1-km MODIS data used in the CERES cloud detection algorithm. In the SW, scattering by adjacent clouds into the clear column can also enhance high-resolution clear-sky fluxes. Contamination of clear pixels in the vicinity of clouds can also occur because of a slight time delay in MODIS detector response (characterized by the instrument point-spread function). As a result, clear-sky radiances adjacent to bright scenes (e.g., clouds) will appear brighter than they really are, thereby artificially raising the clear-sky mean value. Separating these various contributions is an active area in cloud–aerosol interaction research (Koren et al. 2007; Wen et al. 2006; Marshak et al. 2008; Loeb and Schuster 2008). We note that these differences in CERES clear-sky fluxes are much smaller than the 5 W $m^{-2}$ uncertainty in ERBE clear-sky fluxes, which have much larger scene identification errors.

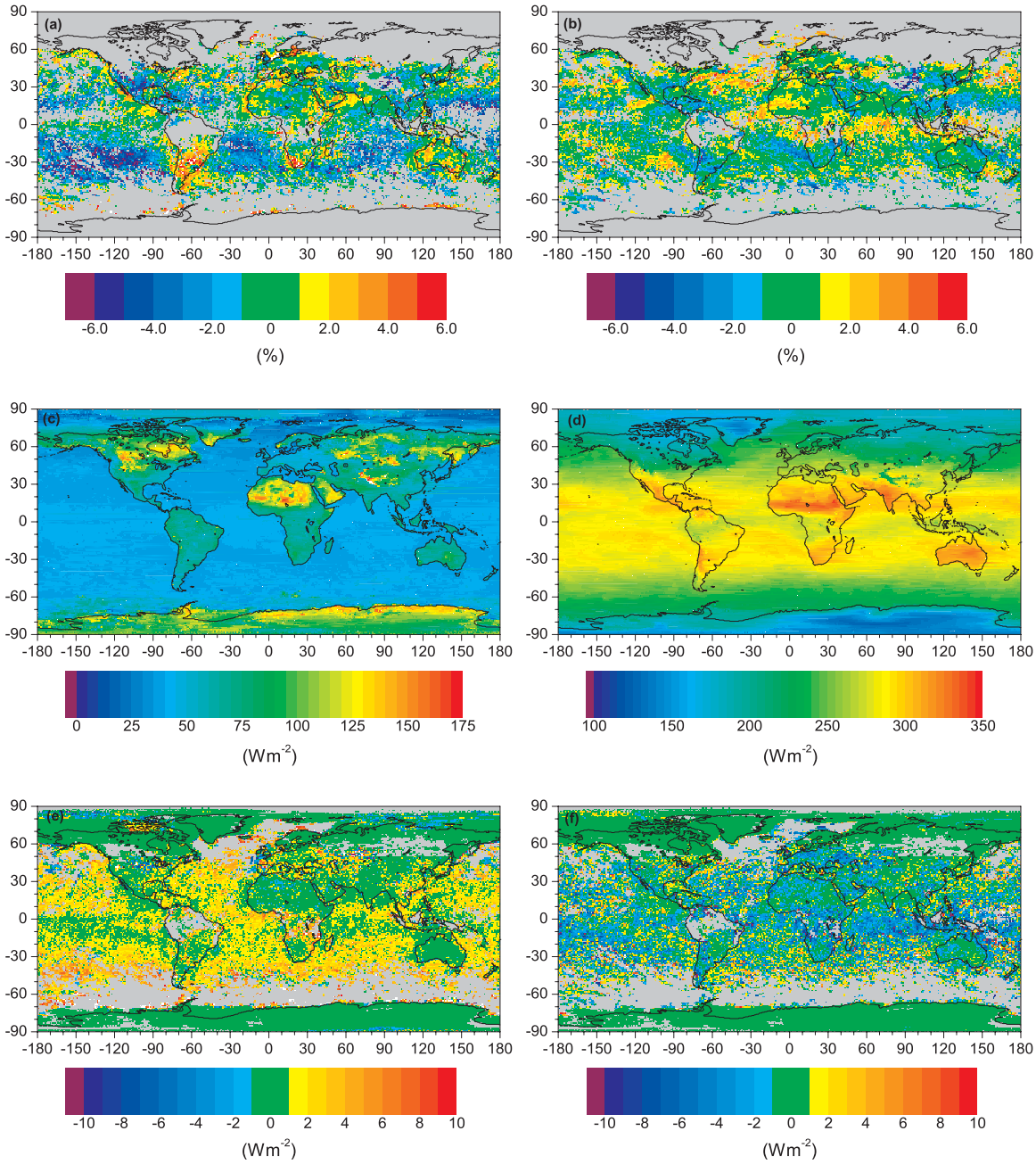


FIG. 3. March 2002 monthly mean results of (a), (b) relative bias error ($1\sigma$) in SW and LW flux due to the narrow-to-broadband conversion for cloud-free CERES footprints; (c), (d) CERES–MODIS clear-sky TOA flux; (e), (f) CERES–MODIS minus CERES-only clear-sky flux difference. Left column shows SW results; right column shows daytime LW results.

The final global mean cloud radiative effect (CRE) values determined from the adjusted all-sky CERES SRBAVG-GEO_Ed2D_rev1 fluxes and the CERES–MODIS clear-sky fluxes (rightmost column in Table 4) are within 1 W m$^{-2}$ of the global mean values from ERBE S-4 (Table 1). The LW CRE exceeds the GEWEX SRB and ISCCP-FD values by 2–3 W m$^{-2}$, whereas the SW CRE value is close to GEWEX SRB, but ~4.5 W m$^{-2}$ smaller than ISCCP-FD. The net CRE from the adjusted CERES data is −17.1 W m$^{-2}$ compared to −17.9 W m$^{-2}$ for ERBE S-4, −19.5 W m$^{-2}$ for GEWEX SRB, and −24.5 W m$^{-2}$ from ISCCP-FD.

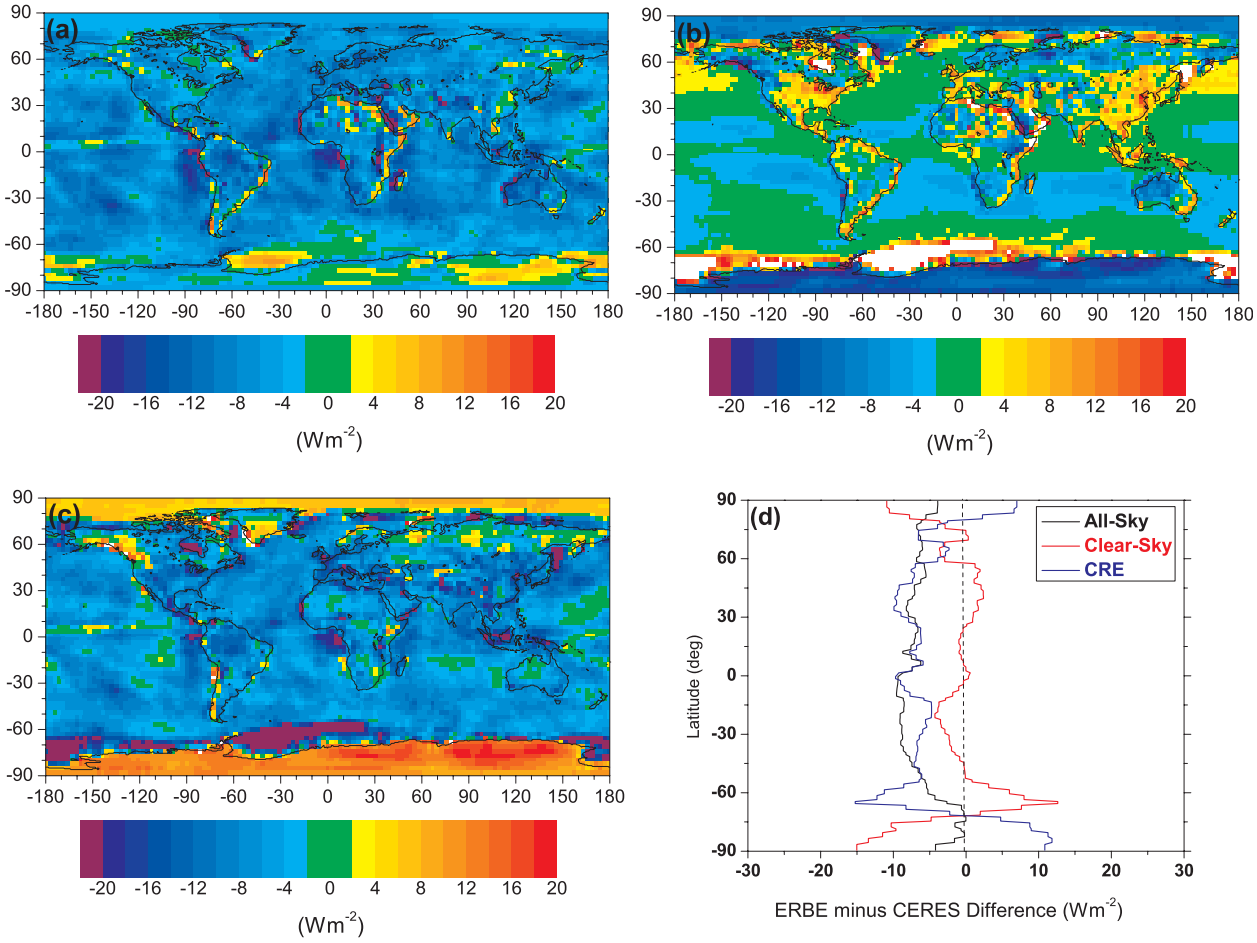


FIG. 4. Adjusted ERBE minus adjusted CERES difference in absorbed solar radiation at TOA for (a) all sky and (b) clear sky; (c) difference in SW CRE. (d) ERBE minus CERES zonal mean differences corresponding to (a)–(c).

## 7. Regional comparisons between adjusted ERBE and CERES radiative fluxes

Figures 4–6 provide direct comparisons between adjusted ERBE fluxes based on Trenberth (1997) and the CERES-EBAF fluxes described in this paper. The Trenberth (1997) adjusted ERBE fluxes have been used by several climate modeling groups for model diagnostic purposes. The period of coverage for the adjusted ERBE data is February 1985 through April 1989, while CERES is from March 2000 through February 2005. While we expect that most of the differences between CERES-EBAF and ERBE are due to the manner in which the TOA flux adjustments were derived, part is undoubtedly due to real differences between the mean states in the two periods. Although the adjusted ERBE dataset distributed by the National Center for Atmospheric Research (NCAR) provide clear-sky ERBE fluxes together with all sky on the same grid, adjustments are only applied to the all-sky fluxes following Trenberth (1997). To compare CERES with ERBE, the CERES 1° × 1° data are interpolated and averaged over a T42 grid.

Figures 4a,b show adjusted ERBE minus CERES-EBAF differences in absorbed solar radiation (ASR) for all sky (Fig. 4a) and clear sky (Fig. 4b), while Fig. 4c shows differences in SW CRE. Figure 4d provides the zonal averages corresponding to Figs. 4a–c. In all-sky conditions, adjusted ERBE ASR is lower than CERES by ~10 W m$^{-2}$ because of the large SW TOA flux adjustments made by Trenberth (1997) (see Table 4). ASR differences for clear sky (Fig. 4b) are smaller over ocean (< 5 W m$^{-2}$) but reach 20 W m$^{-2}$ over North America and East Asia. The largest discrepancies between ERBE and CERES ASR occur over sea ice between 60° and 80°S and over Antarctica. Such large discrepancies are not surprising given the limitations of ERBE over snow and sea ice. Coleman et al. (1997) note that the ice data in ERBE for both the Northern and Southern Hemispheres are based on climatologies from 1973–76. For a

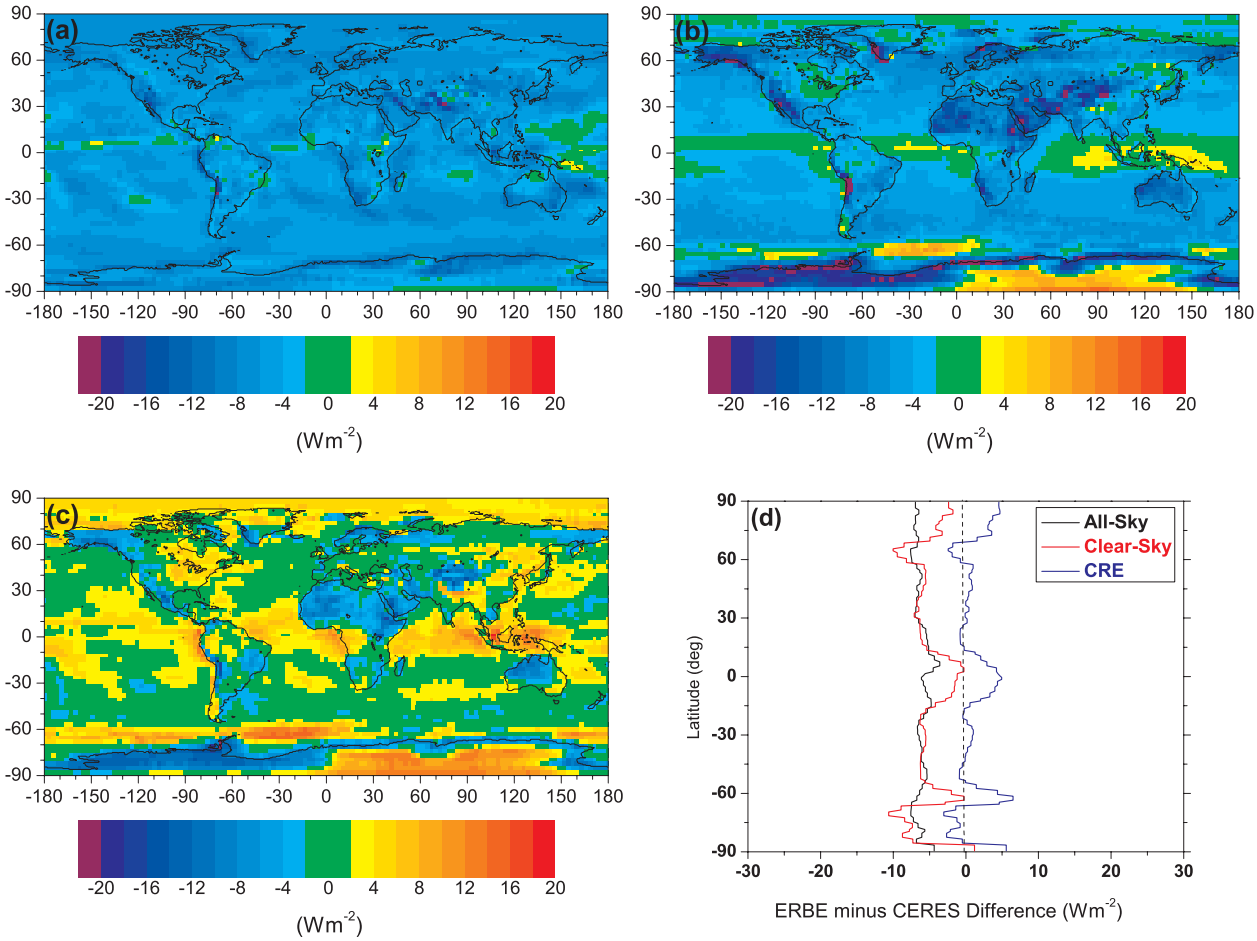


FIG. 5. Same as Fig. 4 but for outgoing LW radiation at TOA.

given month, the minimum sea ice extent during the data period available is assumed, resulting in an underestimation of sea ice coverage and misclassification of clear sea ice as cloud since the scene classification algorithm anticipates a clear scene resembling clear ocean instead of sea ice. CERES correctly identifies cloud-free scenes over sea ice since it uses SSMI-derived snow and sea ice maps updated daily and MODIS spectral measurements to cloud screening. As a result, the 5-yr mean ASR is much too large over sea ice in the ERBE climatology. In the LW (Figs. 5a–d), adjusted all-sky ERBE fluxes are smaller than CERES by 5–10 W $m^{-2}$, whereas in cloud-free conditions ERBE LW fluxes are lower by more than 15 W $m^{-2}$ over some land and desert regions. As a result, differences in LW CRE (Fig. 5c) are positive over ocean and negative over land. These differences nearly compensate one another in the zonal average (Fig. 5d). Finally, all-sky net flux TOA differences (Figs. 6a) are generally negative over most of the tropics with the largest discrepancies occurring in stratus regions off the west coasts of South America and Africa. Differences in both net clear-sky TOA flux and net CRE show rather marked zonal gradients exceeding 20 W $m^{-2}$ in the Southern Hemisphere.

## 8. Summary

Our best estimate of the average global net radiation at the top of the atmosphere (TOA), defined as the difference between the energy absorbed and emitted by the planet, is 0.85 ± 0.15 W $m^{-2}$ (Hansen et al. 2005). Because of uncertainties in absolute calibration and the algorithms used to determine the earth's radiation budget, satellite-based data products show a sizeable imbalance in the average global net radiation at the TOA, ranging from −3 to 7 W $m^{-2}$. A large imbalance in global mean net TOA flux is problematic in many applications that use ERB data. Early attempts to adjust ERB TOA fluxes in order to remove the imbalance in net TOA flux assumed the bulk of the bias is due to

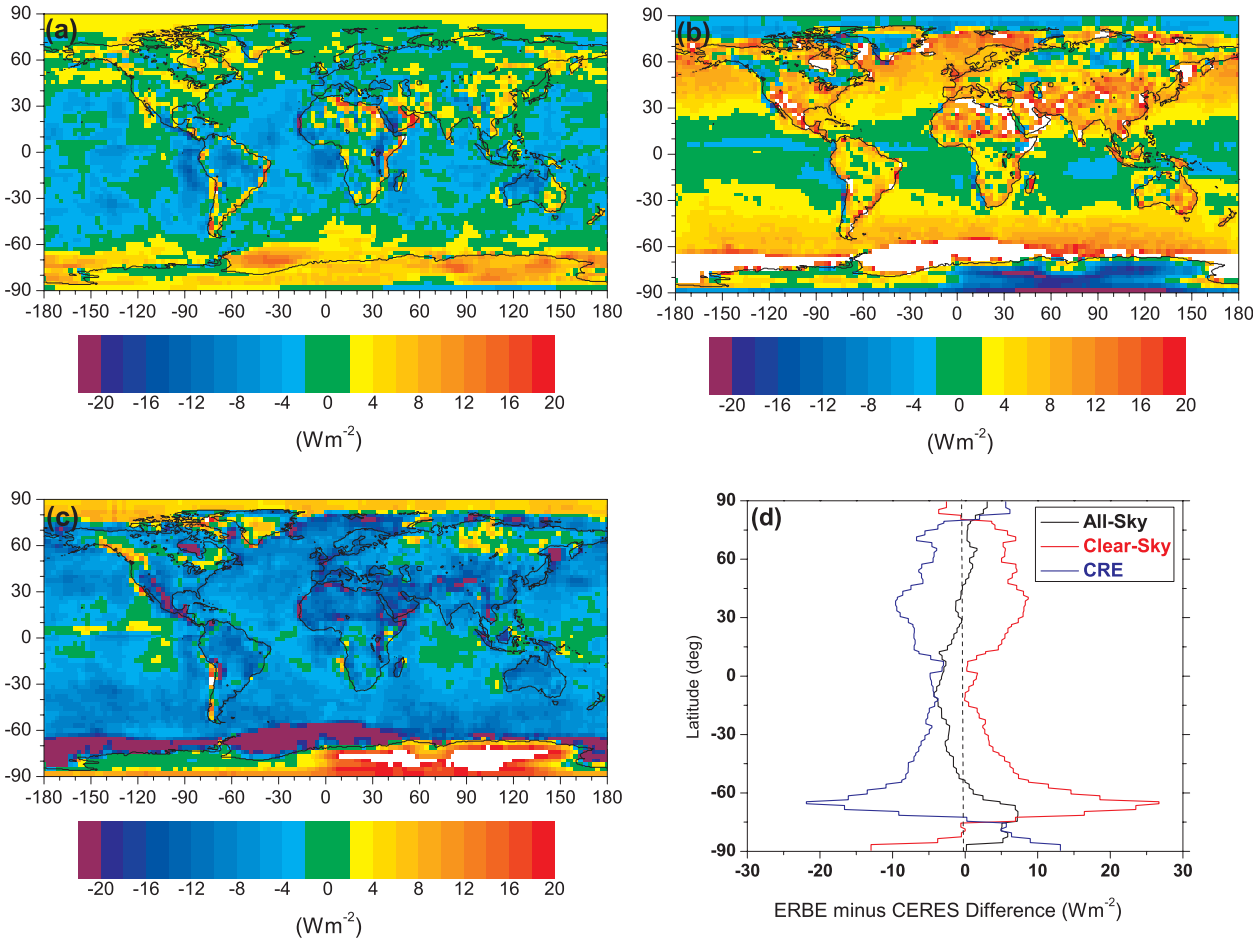


FIG. 6. Same as Fig. 4 but for net downward TOA flux.

sampling and modeling of the diurnal cycle (Trenberth, 1997). Consequently, larger adjustments were made in the SW than in the LW (e.g., Trenberth 1997; Kiehl and Trenberth 1997).

A detailed analysis of the errors and uncertainties that influence the global all-sky net TOA flux from CERES observations reveals that most of the source of bias is not from uncertainty in modeling the diurnal cycle, but rather is from uncertainties in absolute calibration of the measurements. For example, up to 4.2 W $m^{-2}$ of the 6.5 W $m^{-2}$ net TOA flux imbalance in CERES SRBAVG-GEO_Ed2_rev1 product is associated with absolute calibration uncertainty in the SW and TOT channels at the 95% confidence level. As much as 1 W $m^{-2}$ of the imbalance is explained by assuming a solar constant of 1365 W $m^{-2}$ in CERES processing, instead of the newly revised value of 1361 W $m^{-2}$ based on recent total solar irradiance measurements (Kopp et al. 2005). After accounting for the 0.85 W $m^{-2}$ net flux imbalance believed to be real, the remaining error in CERES TOA net flux is associated with smaller uncertainties (e.g., spherical earth assumption, near-terminator flux, unfiltering of CERES radiances, radiance-to-flux conversion, etc.).

While the net TOA flux imbalance from ERBE and CERES ERBE-like are smaller than CERES SRBAVG-GEO (4–5 W $m^{-2}$ compared to 6.5 W $m^{-2}$), this does not mean that the ERBE and CERES ERBE-like data products are more accurate than CERES SRBAVG-nonGEO. The net imbalance in ERBE and CERES ERBE-like is reduced because of systematic errors in the ERBE angular distribution models, which overestimate SW fluxes at mid–high latitudes, causing a fortuitous reduction in net TOA flux. These findings are confirmed by earlier validation studies showing that fluxes from the ERBE ADMs depend systematically upon viewing geometry and cloud type, problems that are largely absent when CERES ADMs are applied.

An objective constrainment algorithm is used to adjust SW and LW TOA fluxes within their range of

uncertainty to remove the inconsistency between average global net TOA flux and heat storage in the earth–atmosphere system. Global monthly mean climatologies of adjusted all-sky and clear-sky SW and LW TOA fluxes are produced for the first 5 yr of CERES *Terra* observations. We refer to the adjusted CERES data as CERES-EBAF, where EBAF stands for Energy Balanced and Filled. The global mean CERES-EBAF SW TOA flux for the first 5 yr of CERES *Terra* (March 2000–February 2005) is 99.5 W m$^{-2}$, corresponding to an albedo of 0.293, and the global mean LW TOA flux is 239.6 W m$^{-2}$. These values differ markedly from the adjusted global means in Trenberth (1997) based on ERBE in which the global mean SW TOA flux is 106.9 W m$^{-2}$ and the LW TOA flux is 234.4 W m$^{-2}$. Zonal differences between adjusted ERBE and CERES-EBAF TOA monthly mean fluxes range from 10 W m$^{-2}$ at low latitudes to 30 W m$^{-2}$ at high latitudes. Regionally, 5-yr mean differences are most pronounced in stratus regions off South America and Africa, and between 60°S and 90°N over sea ice and permanent snow.

A new approach for determining CERES clear-sky TOA flux climatologies is employed that accounts for contributions from cloud-free regions at both the CERES footprint and sub-CERES footprint spatial scales. The approach uses MODIS-derived "broadband" clear-sky fluxes estimated from the cloud-free portions of partly and mostly cloudy footprints. The global mean clear-sky SW TOA flux obtained by including high-resolution clear-sky contributions is 52.9 W m$^{-2}$ in the SW and 269.1 W m$^{-2}$ in the LW. Accounting for the contributions by small-scale clear regions increases the global mean SW TOA flux by 0.9 W m$^{-2}$ in the SW, and decreases the global mean LW TOA flux by 0.3 W m$^{-2}$ compared to global means that only consider cloud-free regions at the CERES footprint scale.

The global mean cloud radiative effect (CRE) from the new CERES-EBAF TOA fluxes is 29.5 W m$^{-2}$ in the LW, −46.6 W m$^{-2}$ in the SW, and the net CRE is −17.1 W m$^{-2}$. These values are within 1 W m$^{-2}$ of CRE values obtained from the unadjusted ERBE S-4 data product (02/85–01/89), in spite of large differences (up to 4.5 W m$^{-2}$) in mean all-sky and clear-sky fluxes. CRE differences reach 7 W m$^{-2}$ when adjusted CERES SW CRE values are compared with those inferred from adjusted all-sky fluxes from Trenberth (1997).

*Acknowledgments.* This research has been supported by the NASA CERES project. The CERES data were obtained from the Atmospheric Sciences Data Center at the NASA Langley Research Center. The authors thank Drs. John Fasullo and Phil Rasch for making the adjusted ERBE data available and the following individuals for helpful discussions: Drs. Kevin Trenberth, Greg Kopp, Kory Priestley, Jean-Louis Dufresne, Robert Pincus, Jerry Potter, Knut von Salzen, and William Collins.

## APPENDIX

### Uncertainty in Net TOA Flux due to Absolute Calibration Uncertainty

The uncertainty in net TOA flux due to absolute calibration uncertainty in CERES is derived from our understanding of uncertainties in the SW and TOT channel measurements. The absolute calibration uncertainty is 2% in the SW channel and 1% in the TOT channel at the 95% confidence level. These uncertainties were determined by a detailed component-by-component analysis of the CERES instrument, in-orbit calibration sources, and the CERES ground calibration facility.

For a global mean SW TOA flux of ≈100 W m$^{-2}$, and a global mean LW TOA flux of 240 W m$^{-2}$, the absolute calibration uncertainty in SW is 2 W m$^{-2}$, and the nighttime LW uncertainty is 2.4 W m$^{-2}$. To determine the uncertainty in LW daytime flux [LW(D)] due to absolute calibration uncertainty, errors in both daytime TOT and SW need to be considered since LW(D) is determined from the difference between the TOT and SW channels:

$$\mathrm{LW}(D) = \mathrm{TOT}(D) - \mathrm{SW}(D), \tag{A1}$$

where TOT($D$) is the daytime TOT channel measurement and SW(D) is the daytime SW channel measurement. Since TOT($D$) and SW($D$) cannot be assumed independent, the error in LW($D$) can be expressed as follows:

$$\delta\mathrm{LW}(D) = [(\delta\mathrm{TOT})^2 + (\delta\mathrm{SW})^2 - 2\{\rho(\mathrm{TOT}, \mathrm{SW})\delta\mathrm{TOT}\delta\mathrm{SW}\}]^{1/2}, \tag{A2}$$

where $\delta$TOT is the uncertainty in TOT channel, $\delta$SW is the uncertainty in the SW channel, and $\rho$ is their correlation coefficient. Based on CERES measurements, $\rho$(TOT, SW) ≈ 0.9 and the instantaneous global mean SW and LW fluxes are ≈ 235 W m$^{-2}$ and ≈ 240 W m$^{-2}$, respectively, for the *Terra* orbit. Assuming a 2% uncertainty in SW and 1% in TOT, Eq. (A2) becomes

$$\delta \mathrm{LW}(D) = \left([0.02(235)]^2 + [0.01(240)]^2 - 2\{0.9[0.02(235)][0.01(240)]\}\right)^{1/2}, \quad \text{(A3)}$$

which yields $\delta \mathrm{LW}(D) = 5\ \mathrm{W\ m^{-2}}$. Therefore, the total 24-h average LW error is $(5 + 2.4)/2 = 3.7\ \mathrm{W\ m^{-2}}$, or $\approx 1.5\%$ of the mean LW flux. For SW, the 24-h average uncertainty is $2\ \mathrm{W\ m^{-2}}$, or $\approx 2\%$ of the mean SW flux. The net TOA flux error due to absolute calibration uncertainty is thus $(2^2 + 3.7^2)^{1/2} = 4.2\ \mathrm{W\ m^{-2}}$.

## REFERENCES


Barkstrom, B. R., 1984: The Earth Radiation Budget Experiment (ERBE). *Bull. Amer. Meteor. Soc.,* **65,** 1170–1185.

Brooks, D. R., E. F. Harrison, P. Minnis, J. T. Suttles, and R. S. Kandel, 1986: Development of algorithms for understanding the temporal and spatial variability of the earth's radiation balance. *Rev. Geophys.,* **24,** 422–438.

Butler, J. J., B. C. Johnson, J. P. Rice, E. L. Shirley, and R. A. Barnes, 2008: Sources of differences in on-orbital total solar irradiance measurements and description of a proposed laboratory intercomparison. *J. Res. Natl. Inst. Stand. Technol.,* **113,** 187–203.

Cavalieri, D., P. Gloerson, and J. Zwally, 1990: DMSP SSM/I daily polar gridded sea ice concentrations. J. Maslanik and J. Stroeve, Eds., National Snow and Ice Data Center, Boulder, CO, digital media.

Coleman, L. H., B. T. Flug, S. Gupta, E. A. Kizer, and J. L. Robbins, 1997: ERBE geographic scene and monthly snow data. NASA Tech. Rep. NASA-97-cr4773, 39 pp.

Comiso, J., 1990: DMSP SSM/I daily polar gridded sea ice concentrations. J. Maslanik and J. Stroeve, Eds., National Snow and Ice Data Center, Boulder, CO, digital media.

Cox, S. J., P. W. Stackhouse Jr., S. K. Gupta, J. C. Mikovitz, T. Zhang, L. M. Hinkelman, M. Wild, and A. Ohmura, 2006: The NASA/GEWEX surface radiation budget project: Overview and analysis. Preprints, *12th Conf. on Atmospheric Radiation*, Madison, WI, Amer. Meteor. Soc., 10.1. [Available online at http://ams.confex.com/ams/pdfpapers/112990.pdf.]

Dewitte, S., L. Gonzalez, N. Clerbaux, A. Ipe, C. Bertrand, and B. De Paepe, 2008: The Geostationary Earth Radiation Budget edition 1 data processing algorithms. *Adv. Space Sci.,* **41,** 1906–1913.

Doelling, D. R., and D. F. Keyes, D. F., Young, B. A. Wielicki, and T. Wong, 2006: The newly released 5-year *Terra*-based monthly CERES radiative flux and cloud product. Preprints, *12th Conf. on Atmospheric Radiation*, Madison, WI, Amer. Meteor. Soc., 9.4. [Available online at http://ams.confex.com/ams/pdfpapers/112727.pdf.]

Fasullo, J. T., and K. E. Trenberth, 2008: The annual cycle of the energy budget: Global mean and land–ocean exchanges. *J. Climate,* **21,** 2297–2312.

Geier, E. B., R. N. Green, D. P. Kratz, P. Minnis, W. F. Miller, S. K. Nolan, and C. B. Franklin, cited 2001: Single satellite footprint TOA/surface fluxes and clouds (SSF) collection document. [Available online at http://asd-www.larc.nasa.gov/ceres/collect_guide/SSF_CG.pdf.]

Hansen, J., and Coauthors, 2005: Earth's energy imbalance: Confirmation and implications. *Science,* **308,** 1431–1435.

Hollinger, J. P., J. L. Peirce, and G. A. Poe, 1990: SSM/I instrument evaluation. *IEEE Trans. Geosci. Remote Sens. Environ.,* **28,** 781–790.

Huang, S., 2006: Land warming as part of global warming. *Eos, Trans. Amer. Geophys. Union,* **87,** 31–44.

Kato, S., and N. G. Loeb, 2003: Twilight irradiance reflected by the earth estimated from Clouds and the Earth's Radiant Energy System (CERES) measurements. *J. Climate,* **16,** 2646–2650.

——, and ——, 2005: Top-of-atmosphere shortwave broadband observed radiance and estimated irradiance over polar regions from Clouds and the Earth's Radiant Energy System (CERES) instruments on Terra. *J. Geophys. Res.,* **110,** D07202, doi:10.1029/2004JD005308.

Keyes, D. F., D. R. Doelling, F. G. Rose, D. A. Rutan, M. L. Nordeen, J. S. Boghosian, and D. F. Young, 2006: The validation of the 5-year *Terra*-based monthly CERES radiative flux and cloud product. Preprints, *12th Conf. on Atmospheric Radiation*, Madison, WI, Amer. Meteor. Soc., P3.1. [Available online at http://ams.confex.com/ams/pdfpapers/112731.pdf.]

Kiehl, J. T., and K. E. Trenberth, 1997: Earth's annual global mean energy budget. *Bull. Amer. Meteor. Soc.,* **78,** 197–208.

Köhl, A., and D. Stammer, 2008: Decadal sea level changes in the 50-year GECCO ocean synthesis. *J. Climate,* **21,** 1876–1890.

Kopp, G., G. Lawrence, and G. Rottman, 2005: The Total Irradiance Monitor (TIM): Science results. *Solar Phys.,* **230,** 129–140.

Koren, I., L. A. Remer, Y. J. Kaufman, Y. Rudich, and J. V. Martins, 2007: On the twilight zone between clouds and aerosols. *Geophys. Res. Lett.,* **34,** L08805, doi:10.1029/2007GL029253.

Levitus, S., J. I. Antonov, J. Wang, T. L. Delworth, K. W. Dixon, and A. J. Broccoli, 2001: Anthropogenic warming of Earth's climate system. *Science,* **292,** 267–270.

Li, Z., and H. G. Leighton, 1991: Scene identification and its effect on cloud radiative forcing in the Arctic. *J. Geophys. Res.,* **96,** 9175–9188.

Loeb, N. G., and N. Manalo-Smith, 2005: Top-of-atmosphere direct radiative effect of aerosols over global oceans from merged CERES and MODIS observations. *J. Climate,* **18,** 3506–3526.

——, and G. L. Schuster, 2008: An observational study of the relationship between cloud, aerosol and meteorology in broken low-level cloud conditions. *J. Geophys. Res.,* **113,** D14214, doi:10.1029/2007JD009763.

——, K. J. Priestley, D. P. Kratz, E. B. Geier, R. N. Green, B. A. Wielicki, P. O. R. Hinton, and S. K. Nolan, 2001: Determination of unfiltered radiances from the Clouds and the Earth's Radiant Energy System (CERES) instrument. *J. Appl. Meteor.,* **40,** 822–835.

——, S. Kato, and B. A. Wielicki, 2002: Defining top-of-atmosphere flux reference level for earth radiation budget studies. *J. Climate,* **15,** 3301–3309.

——, N. M. Smith, S. Kato, W. F. Miller, S. K. Gupta, P. Minnis, and B. A. Wielicki, 2003a: Angular distribution models for top-of-atmosphere radiative flux estimation from the Clouds and the Earth's Radiant Energy System instrument on the Tropical Rainfall Measuring Mission Satellite. Part I: Methodology. *J. Appl. Meteor.,* **42,** 240–265.

——, ——, ——, ——, ——, ——, and ——, 2003b: Angular distribution models for top-of-atmosphere radiative flux estimation from the Clouds and the Earth's Radiant Energy System instrument on the Tropical Rainfall Measuring Mission Satellite. Part II: Validation. *J. Appl. Meteor.,* **42,** 1748–1769.

——, S. Kato, K. Loukachine, and N. M. Smith, 2005: Angular distribution models for top-of-atmosphere radiative flux

estimation from the Clouds and the Earth's Radiant Energy System instrument on the *Terra* satellite. Part I: Methodology. *J. Atmos. Oceanic Technol.,* **22,** 338–351.

——, W. Sun, W. F. Miller, K. Loukachine, and R. Davies, 2006: Fusion of CERES, MISR and MODIS measurements for top-of-atmosphere radiative flux validation. *J. Geophys. Res.,* **111,** D18209, doi:10.1029/2006JD007146.

——, and Coauthors, 2007a: Multi-instrument comparison of top-of-atmosphere reflected solar radiation. *J. Climate,* **20,** 575–591.

——, S. Kato, K. Loukachine, and N. Manalo-Smith, 2007b: Angular distribution models for top-of-atmosphere radiative flux estimation from the Clouds and the Earth's Radiant Energy System instrument on the *Terra* satellite. Part II: Validation. *J. Atmos. Oceanic Technol.,* **24,** 564–584.

Marshak, A., G. Wen, J. A. Coakley Jr., L. A. Remer, N. G. Loeb, and R. F. Cahalan, 2008: A simple model for the cloud adjacency effect and the apparent bluing of aerosols near clouds. *J. Geophys. Res.,* **113,** D14S17, doi:10.1029/2007JD009196.

Matheson, M. A., J. A. Coakley Jr., and W. R. Tahnk, 2006: Multiyear advanced very high resolution radiometer observations of summertime stratocumulus collocated with aerosols in the northeastern Atlantic. *J. Geophys. Res.,* **111,** D15206, doi:10.1029/2005JD006890.

Minnis, P., D. F. Young, S. Sun-Mack, P. W. Heck, D. R. Doelling, and Q. Trepte, 2003: CERES cloud property retrievals from imagers on TRMM, Terra, and Aqua. *Remote Sensing of Clouds and the Atmosphere VIII,* K. P. Schaefer et al., Eds., International Society for Optical Engineering (SPIE Proceedings, Vol. 5235), 37–48.

Priestley, K. J., B. A. Wielicki, R. N. Green, M. P. A. Haeffelin, R. B. Lee, and N. G. Loeb, 2002: Early radiometric validation results of the CERES flight model 1 and 2 instruments onboard NASA's Terra spacecraft. *Adv. Space Res.,* **30,** 2371–2376.

Smith, G. L., 2008: Balancing the Earth's radiation budget. *Proc. 19th Conf. on Probability and Statistics,* New Orleans, LA, Amer. Meteor. Soc., 6.6. [Available online at http://ams.confex.com/ams/pdfpapers/129244.pdf.]

——, R. N. Green, E. Raschke, L. M. Avis, J. T. Suttles, B. A. Wielicki, and R. Davies, 1986: Inversion methods for satellite studies of the Earth's radiation budget: Development of algorithms for the ERBE mission. *Rev. Geophys.,* **24,** 407–421.

Suarez, M. J., 2005: Documentation and validation of the Goddard Earth Observing System (GEOS) data assimilation system, version 4. Tech. Rep. Series on Global Modeling and Data Assimilation, Vol. 26, NASA/TM-2005-104606, 181 pp.

Suttles, J. T., B. A. Wielicki, and S. Vemury, 1992: Top-of-atmosphere radiative fluxes: Validation of ERBE scanner inversion algorithm using *Nimbus-7* ERB data. *J. Appl. Meteor.,* **31,** 784–796.

Trenberth, K. E., 1997: Using atmospheric budgets as a constraint on surface fluxes. *J. Climate,* **10,** 2796–2809.

Wen, G., A. Marshak, and R. F. Cahalan, 2006: Impact of 3D clouds on clear sky reflectance and aerosol retrievals in biomass burning region of Brazil. *Geosci. Remote Sens. Lett.,* **3,** 169–172.

Wielicki, B. A., and R. N. Green, 1989: Cloud identification for ERBE radiative flux retrieval. *J. Appl. Meteor.,* **28,** 1133–1146.

——, R. D. Cess, M. D. King, D. A. Randall, and E. F. Harrison, 1995: Mission to planet earth: Role of clouds and radiation in climate. *Bull. Amer. Meteor. Soc.,* **76,** 2125–2153.

——, B. R. Barkstrom, E. F. Harrison, R. B. Lee III, G. L. Smith, and J. E. Cooper, 1996: Clouds and the Earth's Radiant Energy System (CERES): An earth observing system experiment. *Bull. Amer. Meteor. Soc.,* **77,** 853–868.

Willis, J., D. Roemmich, and B. Cornuelle, 2004: Interannual variability in upper-ocean heat content, temperature and thermosteric expansion on global scales. *J. Geophys. Res.,* **109,** C12036, doi:10.1029/2003JC002260.

Wong, T., B. A. Wielicki, R. B. Lee III, G. L. Smith, K. A. Bush, and J. K. Willis, 2006: Reexamination of the observed decadal variability of the earth radiation budget using altitude-corrected ERBE/ERBS nonscanner WFOV data. *J. Climate,* **19,** 4028–4040.

Young, D. F., P. Minnis, D. R. Doelling, G. G. Gibson, and T. Wong, 1998: Temporal interpolation methods for the Clouds and the Earth's Radiant Energy System (CERES) experiment. *J. Appl. Meteor.,* **37,** 572–590.

Zhang, Y.-C., W. B. Rossow, A. A. Lacis, V. Oinas, and M. I. Mishchenko, 2004: Calculation of radiative fluxes from the surface to top of atmosphere based on ISCCP and other global data sets: Refinements of the radiative transfer model and the input data. *J. Geophys. Res.,* **109,** D19105, doi:10.1029/2003JD004457.